Scientia Iranica F (2021) 28(6), 3776–3785

Sharif University of Technology
Scientia Iranica
Transactions F: Nanotechnology
http://scientiairanica.sharif.edu

The structural, optical, and self-cleaning properties of Mn_3O_4/SnO_2 multilayer thin films deposited using spray pyrolysis technique

S.M. Alduwaib[a,*], Muhannad M. Abd[a], and Ali H.A. Jalaukhan[b]

a. *Department of Sciences, Collage of Basic Education, Al-Mustansiriyh University, Baghdad, Iraq.*
b. *College of Education for Pure Sciences, University of Kerbala, Kerbala, Iraq.*

Received 29 June 2020; received in revised form 22 May 2021; accepted 23 August 2021

KEYWORDS
Tin oxide;
Manganese oxide;
Bilayer;
Self-cleaning;
Spray pyrolysis;
Contact angle.

Abstract. Due to the many applications of self-cleaning surfaces in different industries, the development of self-cleaning coating production methods in a simple and inexpensive way has gained significance among researchers. In this regard, the present study aims to prepare tin oxide and Manganese oxide through sol-gel procedure. Next, (Mn_3O_4/SnO_2) double layers were deposited using spray pyrolysis system on glass substrates. Structural, topology, and optical properties, surface morphology, and wettability characterizations were investigated by X-Ray Diffraction (XRD), UV-Vis spectroscopy, Atomic Force Microscopy (AFM), Field Emission Scanning Electron Microscopy (FESEM), and contact angle, respectively. According to AFM images of Mn_3O_4 thin films, grains were tightly packed and entirely compressed without crack. According to AFM images of SnO_2 films, the values for grain width and Root Mean Square (RMS) roughness are about 242.8 nm and 25.85 mm, respectively. The bilayer images show that the values of grain width and root-mean-square thickness are about 130–220 nm and 20 mm, respectively. In addition, SnO_2 and Mn_3O_4 and SnO_2/Mn_3O_4 films reveal a direct optical band gap and hydrophilicity with water contact angles of 75°, 31°, and 70°, respectively. Owing to the importance and different applications of hydrophilic surfaces, thin layers of metal oxide were produced in a very simple way, among which Mn_3O_4 thin film was characterized by good hydrophilicity.

1. Introduction

Given the possibility of a change occurring in electrical conductivity in a wide range of values and optical transparency, wide-bandgap semiconductors based on Metal Oxides (MO) have received considerable attention [1–3]. Nowadays, such materials have a variety of practical applications such as solar cells, electrochemical devices, and flat panel displays, to name a few [4–6]. In many cases, the amorphous or crystalline structure of MO is mainly composed of oxygen anions and metal cations. Therefore, the defects of the amorphous or crystalline structure are charged and electrically activated, thus exhibiting the acceptor or donor property [7]. It appears that the surface and bulk defects of MO significantly affect the electrical conductivity and charge transfer. In fact, the exact mechanisms of this influence are inexplicable.

MO are used in green technology to destroy different types of harmful and toxic pollutants through photocatalytic activity. MO such as TiO_2 [8,9],

*. *Corresponding author.*
E-mail addresses: Salmansur1975@gmail.com (S.M. Alduwaib); drmmabd@uomustansiriyah.edu.iq (M.M. Abd); alijalaukhan@gmail.com (A.H.A. Jalaukhan)

doi: 10.24200/sci.2021.56298.4650

ZnO [10], WO_3 [11], and Mn_2O_3 [12] have been extensively studied due to their chemical stability, optical gap, and non-toxicity. In order to decrease the pollutants, different inhomogeneous structures have also been synthesized using nano-composites of MoS_2-g-C_3N_4 [13], CuInZnS [14], and Cu_2O nano-particles surrounded by rGO [15]. Among the MO materials, tin oxide is one of the promising tools for self-cleaning applications [16].

Hydrophilicity activity caused by UV radiation is of significance, thus drawing considerable attention [17,18]. The main reason why SnO_2 is widely used as a self-cleaning material is because of its wetness alteration based on ultraviolet radiation [16]. In general, pure SnO_2 is characterized by high photocatalytic efficiency because of its wide bandgap (about 3.6 volts) and high light recombination rate generated by electron-hole pairs.

To date, many researchers have attempted to increase the hydrophobicity of SnO_2 thin layers. Apparently, incorporation of Mn_3O_4 into SnO_2 can improve hydrophilicity [19]. The multilayer thin films gain greater significance for faster development in smaller dimensions of the electronic and optoelectronic devices. Use of multi-layered structures is a sure way to enhance the optical properties of materials. Multi-layered films are well known in many fields owing to their wide range of applications. In bilayer structures, the first layer acts as a substrate for the second layer and this feature changes the entire system. In case the first and second layers are different, the whole system behaves like a new material. Recent research suggests that multi-layered films are used in optical communication systems as well as in piezoelectric applications [20–22]. In this study, SnO_2 and Mn_3O_4 thin films as well as SnO_2/Mn_3O_4 bilayer were deposited on a glass substrate using spray pyrolysis deposition method. After deposition, X-Ray Diffraction (XRD), Field Emission Scanning Electron Microscopy (FESEM), and Atomic Force Microscopy (AFM) analyses of these thin films were carried out to determine the crystallinity as well as the size and topology of the grains. In addition, UV-Vis device was employed to obtain the optical characteristics of the samples. The hydrophilic or self-cleaning properties of the thin films were evaluated by measuring the contact angle of water on the thin films. To the best of the authors' knowledge, no comprehensive investigation of SnO_2/Mn_3O_4 bilayer has been reported so far.

2. Experimental procedures

First, SnO_2 and Mn_3O_4 thin films as well as SnO_2/Mn_3O_4 bilayers were synthesized using sol-gel method. Then, they were deposited using Chemical Spray Pyrolysis (CSP) method from aqueous solutions containing tin chloride and manganese chloride as a precursor and compressed air as a carrier gas. Under spray conditions, the substrate temperature ranges from 450 to 550°C; the distance of the nozzle to substrate ranges from 28 to 30 cm; and solution flow rate is 4–3 ml/min. Glass slides were cleaned by ultrasonics for 30 min and then, they were used as the substrate for nano-material growth. The glass substrates were then placed on a solid conductive surface to provide proper heating to the layers. The parameters used in the deposition process are presented in Table 1. A schematic design of the spray pyrolysis device is presented in Figure 1. The deposited thin films contain XRD analyses using the D8 Advance Bruker YT diffractometer via CuKα radiation at $\lambda = 1.5418$Å and at 2θ values between 5° and 80°, FESEM using the MIRA3TESCAN-XMU model, and AFM using Full Plus model from Ara-research Company. The optical absorption spectrum was obtained by UV-Vis device using U3500 model in the wavelength range of 200 to 700 nm. The measurement of the hydrophobic or self-cleaning property was also performed by studying the contact angle of water drops on the films in ambient conditions at 25°C. For one sample, water drops were placed in three different positions and their mean was considered as the contact angle [23].

Table 1. The deposition parameters of the thin films for the spray pyrolysis process.

Deposition parameters	Value
Substrate	Glass
Solution flow rate	3–4 mL/min
Carrier gas	Compressed air
Substrate temperature	450–55°C
Nozzle-substrate distance	38 cm

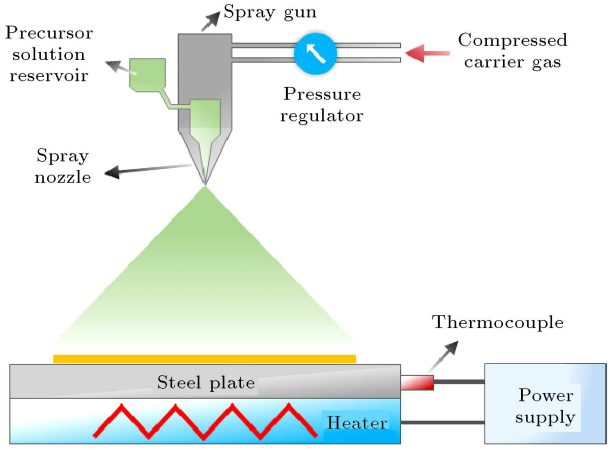

Figure 1. The schematic design of spray pyrolysis device.

3. Results and discussion

3.1. X-Ray Diffraction (XRD)

The crystalline structure of SnO_2 film was demonstrated using XRD via CuKα radiation ($\lambda = 1.5406$Å).

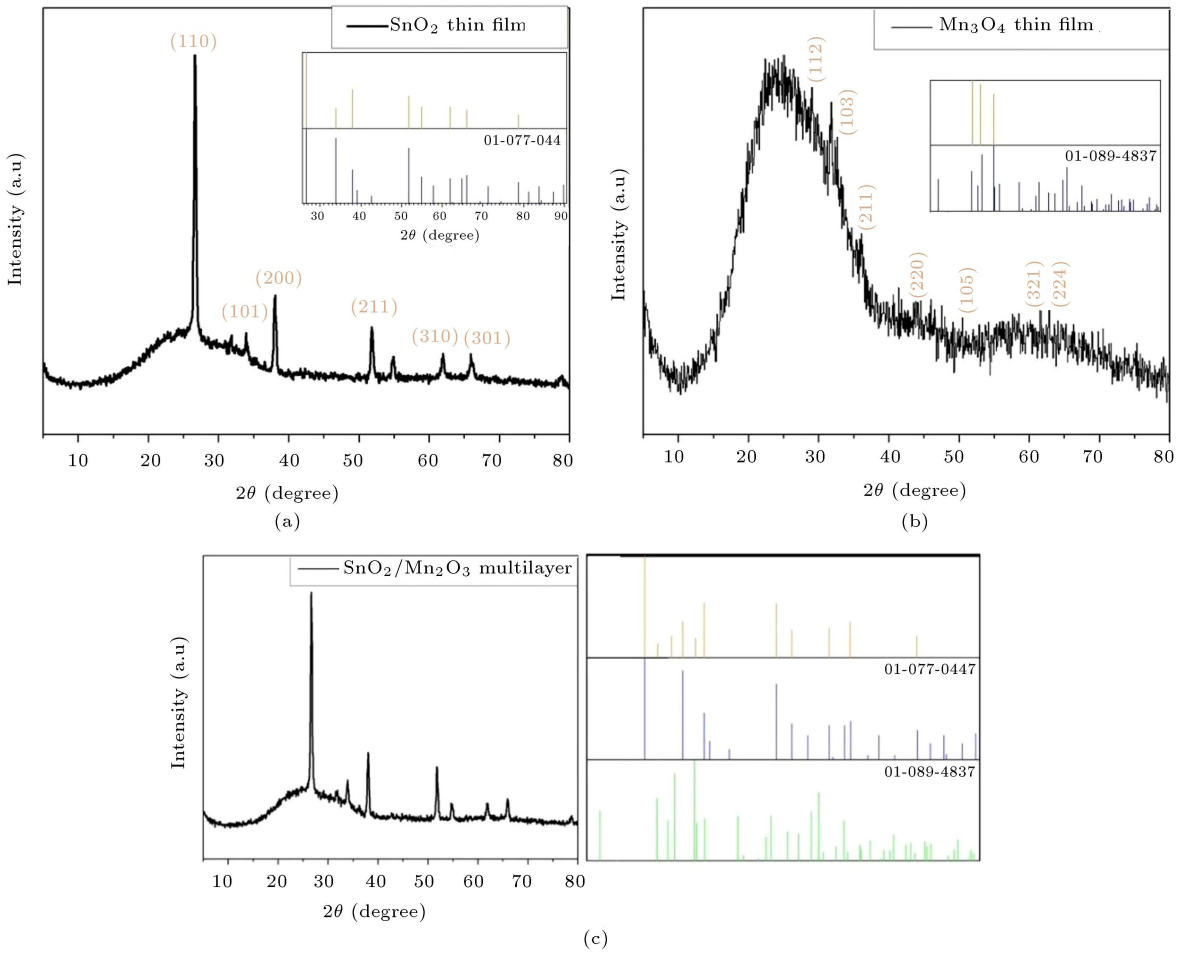

Figure 2. X-Ray Diffraction (XRD) pattern of (a) SnO_2 thin film, (b) Mn_3O_4 thin film, and (c) SnO_2/Mn_3O_4 bilayers. The insets of pictures show the identified phases.

The range of 2θ angles was chosen from 5° to 80°. Figure 2(a) illustrates the XRD pattern of SnO_2 thin film deposited at 500°C. As seen in the XRD pattern, SnO_2 thin film appears to have a polycrystalline structure with a tetragonal cassiterite crystalline phase, in accordance with JCPDS card No. 41-1445 [24]. The diffraction peaks are related to the planes of (110), (101), (111), (211), (220), (221), and (112) which correspond to the tetragonal crystalline structure of SnO_2 film. The values for lattice parameters of $a = b =$ 4.71Å and $c = 3.19$Å were determined, corresponding to the reported bulk values ($c = 3.1871$Å and a = 4.7382Å) [25]. The average grain size was measured using Scherrer formula [26]:

$$D = K \times \lambda / \beta COS\theta, \quad (1)$$

where D is the average grain size of the nano-particles, β is (FWHM) values of the diffraction peaks, $\lambda =$ 1.5406Å, and K equals 0.9. The crystalline sizes of the films were between 18 and 40 nm and the grain size was small, hence very severe grain boundary scattering and low mobility, pointing to the resistance of the layers. The small size of the grain creates much surface energy.

Figure 2(b) shows the XRD of Mn_3O_4 deposited thin film at 450°C in the previous deposition conditions. According to this figure, the deposited films at 450°C exhibit a low crystalline degree due to the powdery nature of its surface. The XRD pattern of Mn_3O_4 is indicative of poor crystallization, affected by saturation reaction and re-evaporation of atomic species during spraying from the nozzle to the layer surface [27]. Diffraction peaks are related to the planes of (101), (112), (103), (211), (004), and (220) with the preferred orientation of (103), being indicative of their low crystalline degrees. The positions of the obtained diffraction peaks were determined and compared with the standard card. It was found that the mentioned outcome was in good agreement with the standard values of JCPDS-24-0734, thus confirming the formation of Mn_3O_4 tetragonal phase (with I41/amd space group).

Figure 2(c) depicts the XRD pattern of SnO_2/Mn_3O_4 bilayers simultaneously deposited on a

substrate at 500°C in the previous deposition conditions. As observed in this figure, the polycrystalline structure is well specified and simultaneous presence of two phases of SnO_2 and Mn_3O_4 can be confirmed using X'Pert software, which is in agreement with the standard values of 01-077-0447 for SnO_2 and 01-089-4837 for Mn_3O_4.

The size of SnO_2/Mn_3O_4 multilayer grains was calculated using Scherrer equation. The crystalline sizes of the films ranged between 15 and 45 nm.

3.2. FE-SEM and cross-section analysis

FESEM images of SnO_2 thin films deposited on the glass substrate at different points with two magnifications are shown in Figure 3(a). The thin layers are uniform with continuous grain distribution and they contain no crack. The presence of large, polyhedral-like grains in this figure confirms that the crystals are formed by a tightly-packed type of growth. Random distribution of grains causes scattering, thus reducing the transmission. The formed grains were already reported by Babar et al. [28,29].

The surface morphology of Mn_3O_4 deposited using a spray pyrolysis device on the glass substrate was investigated using FESEM images with different magnifications, as illustrated in Figure 3(b). These images show the 3D growth of the completely spherical grains of Mn_3O_4. These grains are very uniform, yet entirely separated from each other.

According to FESEM images, the substrate surface is uniformly covered with fine grains of Mn_3O_4. The grain size ranges from 20 to 30 nm, which is in agreement with the specified grain size of XRD peak.

FESEM image of the morphology of SnO_2/Mn_3O_4 sample is shown in Figure 3(c). This sample is characterized by a rough, porous polycrystalline structure with polyhedral-like grading. As observed, the porosity rate in this sample decreased upon increasing Mn_3O_4. Figure 3(d) represents the image of the cross-section of SnO_2/Mn_3O_4. The thickness of each film was found to be about 50–70 nm and Mn_3O_4 nano-particles were well aggregated in the top layer.

3.3. AFM analysis

AFM is a common method for investigating the surface morphology at a very high resolution, even with molecular or atomic precision. Surface morphology was evaluated using an atomic force microscope. Root Mean Square (RMS) of the roughness of thin layers was derived from AFM image data. Figure 4(a)–(c) shows 2- and 3-dimensional AFM images with a size

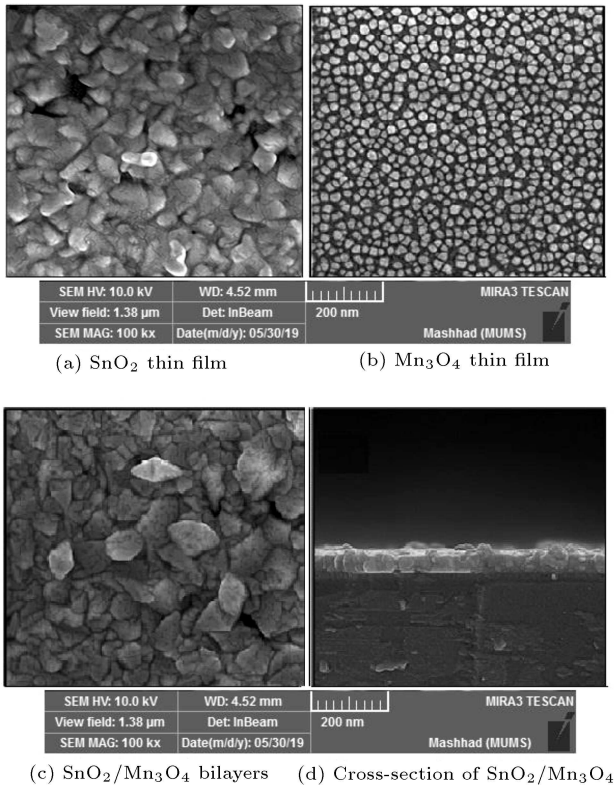

(a) SnO_2 thin film (b) Mn_3O_4 thin film

(c) SnO_2/Mn_3O_4 bilayers (d) Cross-section of SnO_2/Mn_3O_4

Figure 3. Field Emission Scanning Electron Microscopy (FESEM) images of (a) SnO_2 thin films, (b) Mn_3O_4 thin films, (c) SnO_2/Mn_3O_4 bilayers, and (d) cross-section of SnO_2/Mn_3O_4.

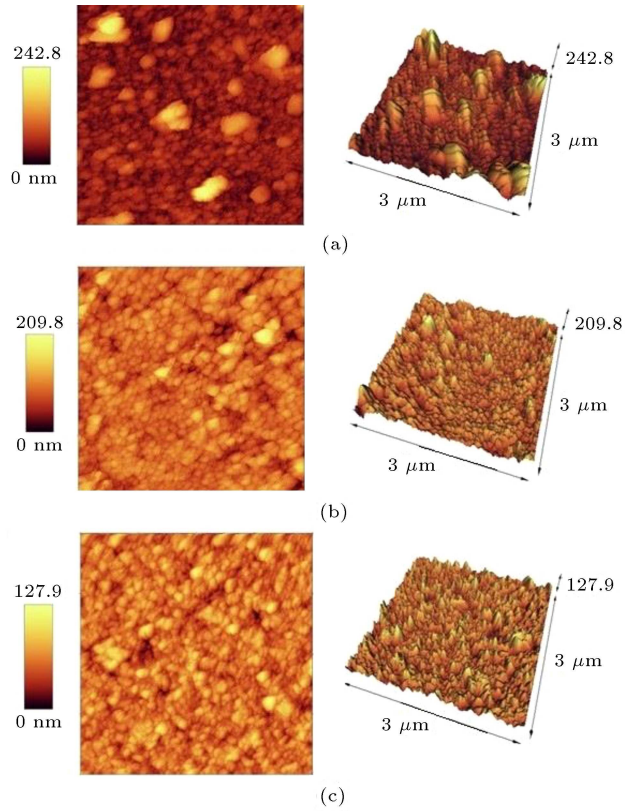

Figure 4. Two- (left) and three-dimensional (right) Atomic Force Microscopy (AFM) images of (a) SnO_2 thin films, (b) Mn_3O_4 thin films, and (c) SnO_2/Mn_3O_4 bilayers.

of 2×2 μm for SnO_2 and Mn_3O_4 thin films as well as SnO_2/Mn_3O_4 multilayer. The surface roughness for the films is 17, 25, and 22 nm, respectively, which is unavoidable because of the 3D growth of the film [30–32]. Two- and three-dimensional images were used to estimate the grain size and orientation, respectively.

The AFM image was studied to observe the surface morphology of Mn_3O_4 with the RMS thickness of about 17.8 mm. Based on the micrograph, it can be seen that the thin film containing Mn_3O_4 grains is tightly packed, entirely compressed, and devoid of crack. AFM study on the morphology of SnO_2 film indicates that the base width of grain was 200.8 nm and RMS roughness was 25.85 mm. Activities of atoms that moved on the surface and grew towards low-energy positions can be considered as the cause of the observed increase in the grain size. In addition, as the roughness of SnO_2 film increased, the hydrophobicity level increased, too. Study of AFM images of SnO_2/Mn_3O_4 multilayer thin film shows that the width grain and RMS thickness in this sample are about 130–220 nm and 20 mm, respectively. This seems to be inconsistent with Wenzel's equation for hydrophilic surfaces. The Wenzel equation predicts that an increase in the surface roughness reduces the contact angle. However, it should be noted that the wetting ability of the surface is controlled by surface roughness and surface energy.

3.4. Optical properties

The optical transmittance of SnO_2 and Mn_3O_4 thin films as well as SnO_2/Mn_3O_4 bilayer was obtained using UV-Vis spectrophotometer at room temperature. SnO_2 thin films, which were very transparent, were placed on the glass substrate mainly due to the formation of Fermi level in the conduction band [33]. Figure 5(a) shows the optical transmission spectrum of this thin film in the visible light region (300–800 nm). According to this figure, SnO_2 film has the highest transmission rate ranging from 650 to 800 nm and the maximum transmission rate of 95%. This is in agreement with the results reported by other researchers [34] in which SnO_2 films indicate higher transmission than 80%. The waves shown in the transmission spectrum may result from light interference since they represent the waveforms that are the characteristics of light interference [35].

The optical transmittance spectrum of Mn_3O_4 thin films obtained from UV-Vis spectroscopy at wavelengths of 300–800 nm is illustrated in Figure 5(b). The transmittance spectrum of Mn_3O_4 thin film at 350 nm increased from 35% to 85% in the wavelength range of 550–800 nm.

The optical transmission in the thin film of SnO_2/Mn_3O_4 bilayer, deposited on the glass substrate in the wavelength range of 350–800 nm, is shown in Figure 5(c). The transmittance in this film reached 85% in the wavelength range of 600–800 nm. This transmittance rate is very promising because it has the ideal optical properties.

According to the reports [36], the electron can be transferred, whether directly or indirectly, from the valence to the conduction band by absorbing the photon energy. The bandgap energy of the film can be almost determined by the transmittance spectrum. The absorption coefficient was calculated by the Tauc relation [37] as follows:

$$\alpha h\nu = B(h\nu - E_g)^2, \tag{2}$$

where B is the constant with different values for different transmittances, E_g the gap energy, $h\nu$ the photon energy, and m the power, all with the hypothetical values of 1.2, 3.2, 2, and 3 and depend on the electronic transmission. By drawing the $(\alpha h\nu)^n$ diagram versus $h\nu$, the optical bandgap energy of the films can be determined. The diagram is plotted by $n = 1/m$ with the assumption that $n = 2$ is allowed for direct transmittance [38]. For SnO_2 and Mn_3O_4 thin films as well as SnO_2/Mn_3O_4 bilayer samples, the value of $2n$ was selected (for direct bandgap transition), as shown in Figure 6(a)–(c) [39] [40]. As observed in Figure 6(a), the optical bandgap energy of SnO_2 thin film is about 3.1 eV at the substrate temperature of

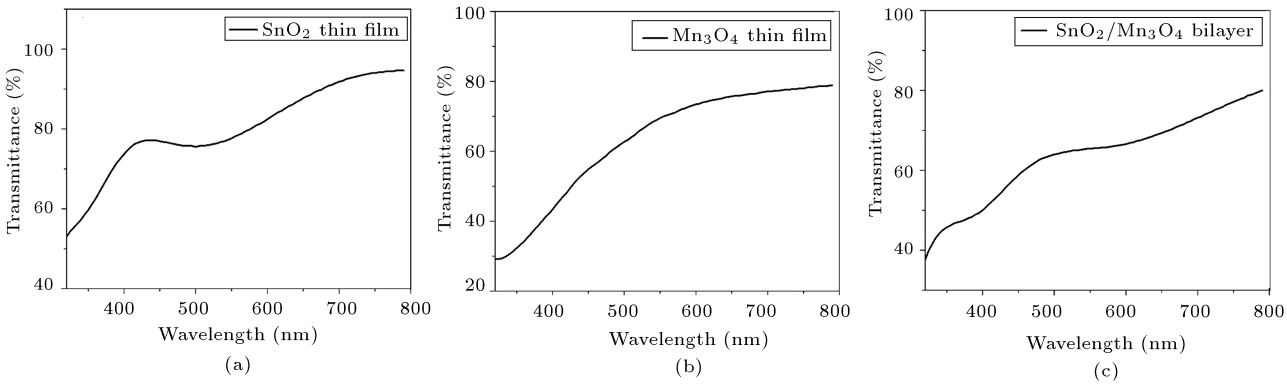

Figure 5. The optical transmittance spectra of (a) SnO_2 thin films, (b) Mn_3O_4 thin films, and (c) SnO_2/Mn_3O_4 bilayers.

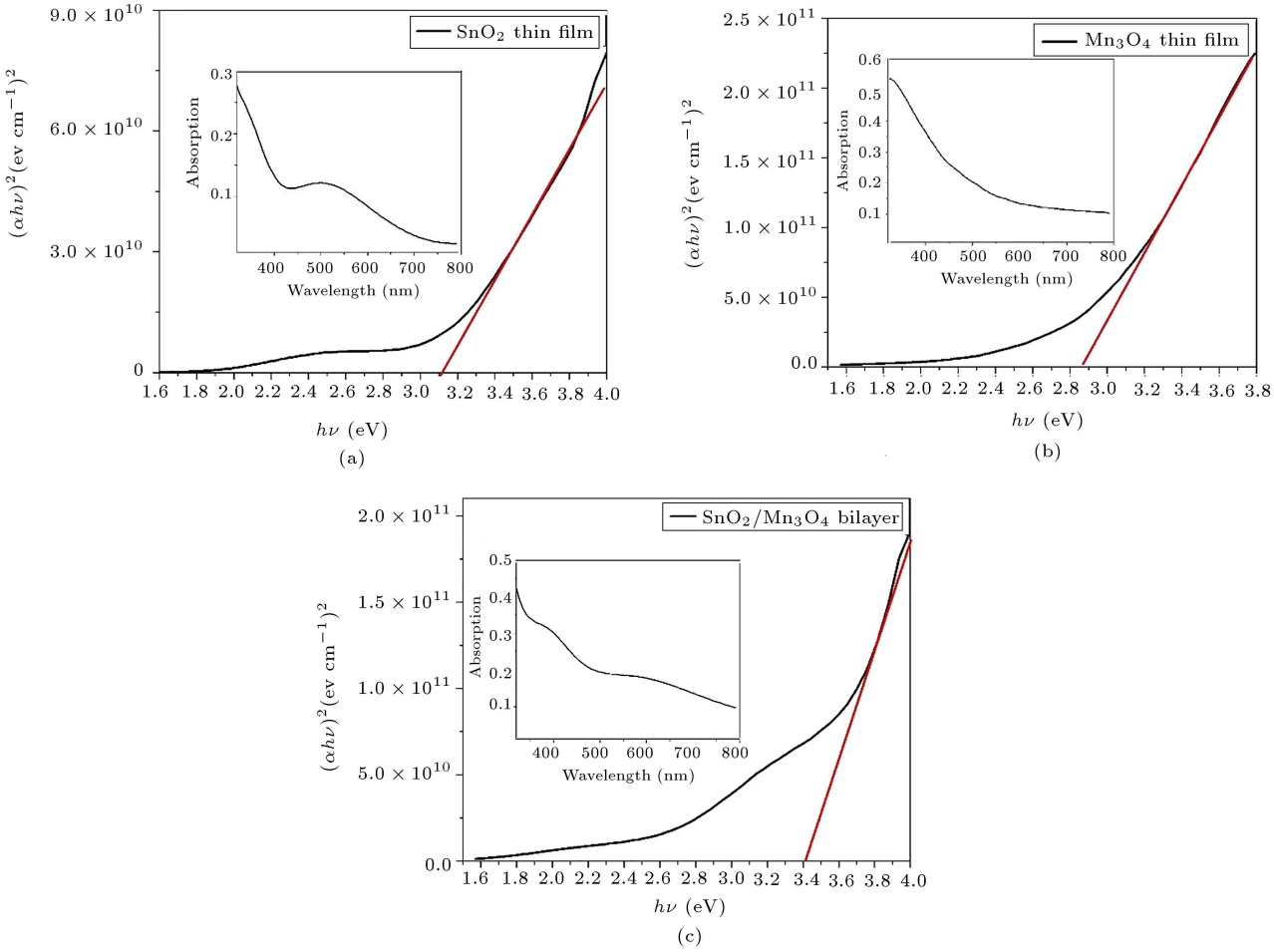

Figure 6. The $(\alpha h\nu)^2$ versus $h\nu$ graphs of (a) SnO_2 thin films, (b) Mn_3O_4 thin films, and (c) SnO_2/Mn_3O_4 bilayers.

500°C. According to other studies [41], as the substrate temperature increased, the energy gap decreased. Of note, except for the removal of oxygen vacancies, high temperatures would cause more concentration of the oxygen atoms in the interstitial (intermediate) sites. The oxygen interstitial sites are caused by a separate band defect in the bandgap region, and the high temperature in the substrate reduces the value of E_g in SnO_2 film [42]. The absorption curve of Mn_3O_4 thin film prepared at 450°C in the region between 300 and 800 nm is illustrated in Figure 6(b). The spectrum exhibits significant absorption in the visible region, thus pointing to its application as an adsorbent. The optical gap energy of Mn_3O_4 thin layer was found to be 2.83 eV, which is consistent with those from other studies [43].

The absorption spectrum of SnO_2/Mn_3O_4 bilayer sample is shown in Figure 6(c). The highest absorption peak for this film occurs at 380 nm. The bandgap energy of SnO_2/Mn_3O_4 bilayer is observed at about 3.4 eV, which is higher than SnO_2 and Mn_3O_4 films. As the number of layers increased, a blue shift was observed at the absorption edge. The reason for this increase in the bandgap of the samples can be attributed to the increase in the number of layers [35]. Multilayer structures are good candidates for optical applications.

The optical constants of SnO_2 and Mn_3O_4 thin films as well as SnO_2/Mn_3O_4 bilayer with the refractive index (n) and extinction coefficient (k) were computed by the transmittance and reflection curves. The refractive index of the samples can be calculated using the following equation [44,45]:

$$n = n_s(1 + \sqrt{R}/1 - \sqrt{R})^{1/2}, \tag{3}$$

where n_s is the refractive index of substrate and R the reflection. The refractive index of the glass substrate is equal to 1.51. The extinction coefficient k can be calculated through the following equation [41]:

$$k = \alpha\lambda/2\pi, \tag{4}$$

where α is the absorption coefficient of the films and λ the wavelength of light. Figures 7(a)–(c) show the refractive index changes, and Figures 8(a)–(c) show the extinction coefficient for these samples in terms of

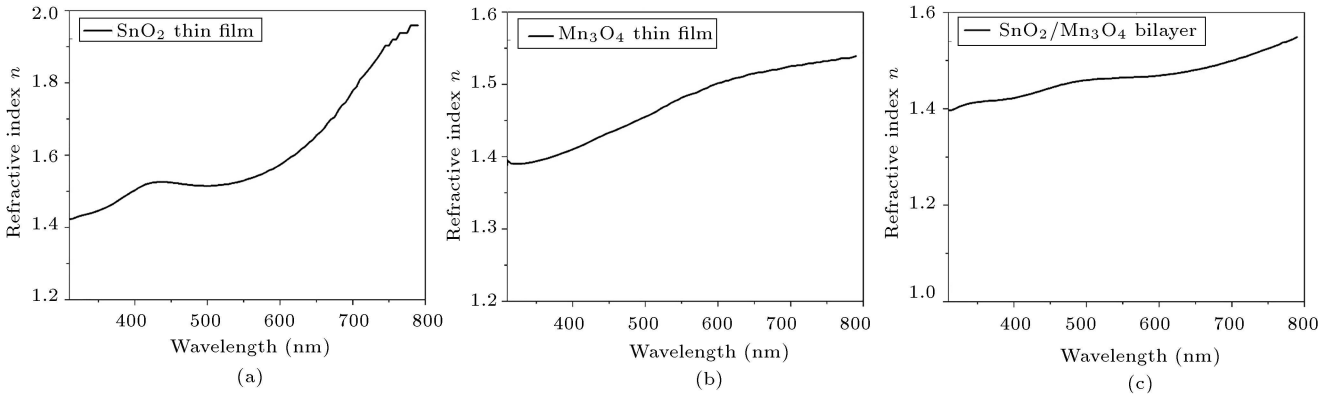

Figure 7. Dispersion of refractive index n with wavelength for (a) SnO_2 thin films, (b) Mn_3O_4 thin films, and (c) SnO_2/Mn_3O_4 bilayers.

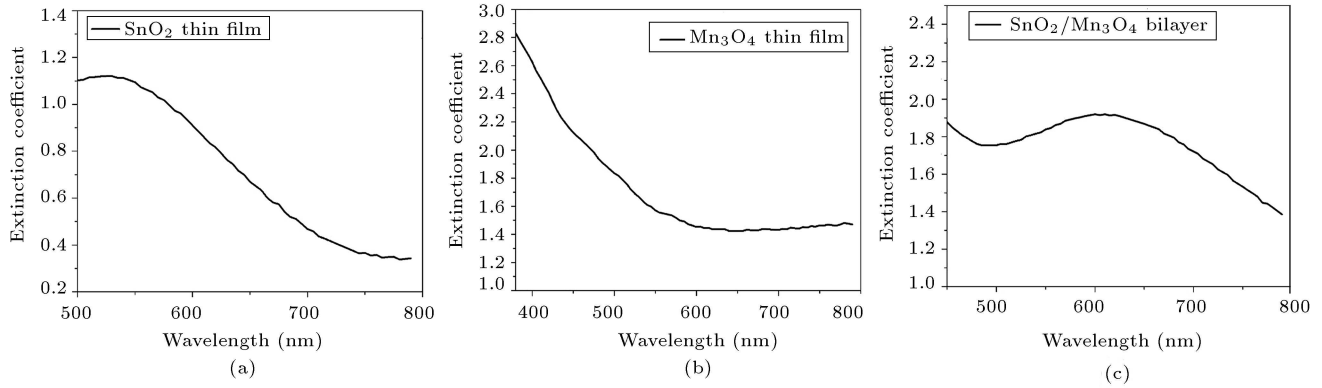

Figure 8. Extinction coefficient curve versus wavelength for (a) SnO_2 thin films, (b) Mn_3O_4 thin films, and (c) SnO_2/Mn_3O_4 bilayers.

wavelength. As observed in these figures, the refractive index of the films follows an increasing trend with the wavelength that corresponds to the behavior of the reflection spectrum. The refractive index value in SnO_2 films at $\lambda = 450$ nm increased from about 1.5 to 2.1 [46]. The value of n for Mn_3O_4 film at $\lambda = 550$ nm also demonstrated an increasing trend from 1.39 to 1.58. With the simultaneous deposition of SnO_2/Mn_3O_4 bilayer, as illustrated in this figure, the increasing trend of the refractive index continued up to 1.7. According to Figure 8(a)–(c), the extinction coefficient for SnO_2 film at 500 nm is about 1. This value for Mn_3O_4 film and SnO_2/Mn_3O_4 bilayer at 600 nm is about 2 and 1.8, respectively.

3.5. Hydrophilic properties

Wetting of a solid surface with water depends on the relationship between the surface tensions (solid/air, water/solid, and water/air). The contact angle between the water drops and surface determines the ratio between these tensions. In the case of complete wetting of the surface, the contact angle is zero in degree and the contact angle of 180° shows that the surface is not completely wet. The surface wettability requires the interaction between the liquid and solid surface.

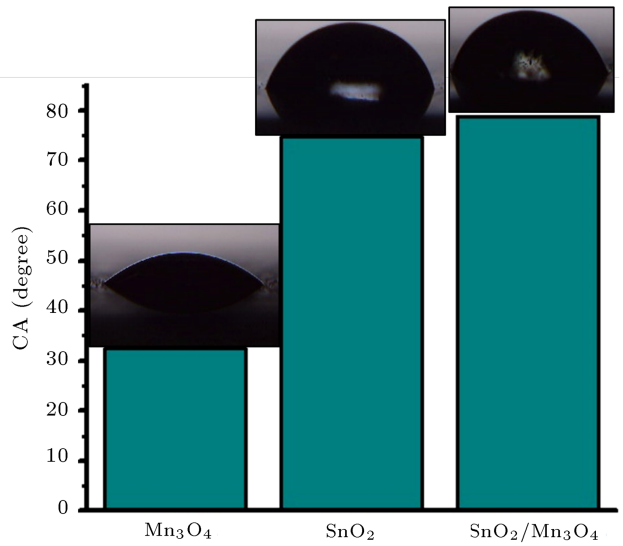

Figure 9. Contact angle measurement for (a) SnO_2 thin films, (b) Mn_3O_4 thin films, and (c) SnO_2/Mn_3O_4 bilayers.

Figure 9 shows the contact angle of the water drops of SnO_2 and Mn_3O_4 thin films as well as SnO_2/Mn_3O_4 bilayer deposited on a glass substrate. The contact angle of about 75° for SnO_2 film is characterized by

an average of five repetitions. Water molecules disrupt this bond by forming new hydroxyl groups. In dark conditions, hydroxyl groups are gradually repelled from the surface. The reason for this increase in hydrophilicity can be related to an increase in hydroxyl groups on the SnO_2 surface [47,48]. According to Figure 9, water is flatly placed on the surface of Mn_3O_4 film with a mean contact angle of 31°, instead of forming a drop. This property is attributed to the nano-crystalline nature, which is expected to have a high energy level. Hydrophilic nano-crystalline materials are the main requirement for electrode materials of superconductors. This property is useful for the close connection between the aqueous electrolyte and the film surface for the application of superconductors. A similar type of observation was reported by Mane et al. [49]. The shape of the drop for SnO_2/Mn_3O_4 bilayer is illustrated in Figure 9. The contact angle between the formed water drop and the surface of this film is about 70°. The presence of Mn_3O_4 film on the substrate of SnO_2 film enhances the hydrophilic properties of the film.

4. Conclusions

The present study managed to investigate the morphological, structural, optical, and self-cleaning properties of SnO_2 and Mn_3O_4 thin films and Mn_3O_4/SnO_2 bilayer prepared using spray pyrolysis system on glass substrates. The X-Ray Diffraction (XRD) pattern of SnO_2 and Mn_3O_4 thin films demonstrated the polycrystalline structure with tetragonal cassiterite and tetragonal hausmannite structures, respectively. Field Emission Scanning Electron Microscopy (FE-SEM) images indicated the polyhedral-like grains for SnO_2 thin films and these images in the case of Mn_3O_4 film demonstrated that the substrate surface was uniformly covered with spherical beads-like architecture. In addition, FESEM images of the morphology of SnO_2/Mn_3O_4 bilayer showed a porous polycrystalline structure with the polyhedral-like grading. The cross-section of SnO_2/Mn_3O_4 was indicative of the thickness of each film which was found to be about 50–100 nm. According to Atomic Force Microscopy (AFM) images of Mn_3O_4 thin films, grains were tightly packed, entirely compressed, and devoid of crack. AFM images for SnO_2 films showed that the width of grain was 242.8 nm and Root Mean Square (RMS) roughness was 25.85 mm. According to these images for the bilayer, the grain width was about 130–220 nm and root-mean-square thickness was about 20 mm. Both SnO_2 and Mn_3O_4 films and SnO_2/Mn_3O_4 bilayer had a direct optical bandgap. The optical bandgap energies for SnO_2 and Mn_3O_4 thin films as well as SnO_2/Mn_3O_4 bilayer were 3.1, 2.83, and 3.4 eV, respectively. The contact angle of the water drops of SnO_2 and Mn_3O_4 thin films and SnO_2/Mn_3O_4 bilayer was characterized by contact angle measurement. Hydrophilicity rates with water contact angle of SnO_2 and Mn_3O_4 films and SnO_2/Mn_3O_4 bilayer were 75°, 31°, and 70°, respectively. According to the obtained results, the Mn_3O_4 thin layer exhibited good hydrophilicity among the synthesized layers. Hydrophilicity was also employed to achieve the desired effect for many applications such as anti-fog coatings, biomedical, filtration, heat pipes, etc.

References

1. Karazhanov, S.Zh. "Phase stability, electronic structure, and optical properties of indium oxide polytypes", *Phys. Rev. B*, **76**(7), pp. 075129–075132 (2007).
2. Medvedeva, J.E., Buchholz, D.B., and Chang, R.P.H. "Recent advances in understanding the structure and properties of amorphous oxide semiconductors", *Adv. Electron. Mater.*, **3**(9), pp. 1700082–1700099 (2017).
3. Korotin, M.A. "Magnetic state of iron impurity ions in In_2O_3", *JETP Lett.*, **108**(8), pp. 537–542 (2018).
4. Granqvist, C.G., *Handbook of Inorganic Electrochromic Materials*, Elsevier Science, Amsterdam (1995).
5. Kompany, A., Ghanbari Shohany, B., and Khorsand Zak, A. "Characterization and optical properties of Cadmium Telluride nanopowders synthesized via hydrothermal method", *J of Research on Many Body Systems*, **6**(12), pp. 71–78 (2017).
6. Freeman, A.J. "Chemical and thin-film strategies for new transparent conducting oxides", *MRS Bull.*, **25**(8), pp. 45–51 (2000).
7. Mezdrogina, M.M. "Parameters of ZnO films with p-type conductivity deposited by high-frequency magnetron sputtering", *Semiconductors*, **51**(5), pp. 559–564 (2017).
8. Jalaukan, A.H.A., Aldowaib, S.A.M., Hameed, A.S., Ghanbari Shohany, B., Etefagh, R., and Khorsand Zak, A "Photo catalytic activity, antibacterial effect, and self cleaning properties of TiO_2/GO thin films", *Iranian Journal of Materials Science and Engineering*, **16**(4), pp. 53–62 (2019).
9. Yu, H., Li, X., Zheng, J.S.J., and Xu, W. "Photocatalytic activity of TiO_2 thin film non uniformly doped by Ni", *Mater. Chem. Phys.*, **97**(1), pp. 59–63 (2006).
10. Motevalizadeh, L., Ghanbari, B., and Ebrahimizadeh, M. "Effects of Mn doping on electrical properties of ZnO thin films", *Modern Physics Letters B*, **30**(4), pp. 1650024–36 (2016).
11. Qamar, M., Yamani, Z.H., Gondal, M.A., and Alhooshani, K. "Synthesis and comparative photocatalytic activity of Pt/WO_3 and Au/WO_3 nanocomposites under sunlight-type excitation", *Solid State Sci.*, **13**(2), pp. 1748–1758 (2011).

12. Qurashi, A., Zhong, Z., and Alam, M.W. "Synthesis and photocatalytic properties of α-Fe_2O_3 nano ellipsoids", *Solid State Sci*, **12**(5), pp. 1516–1519 (2010).

13. Wen, M., Xiong, Q.T., Zang, Z.G., Wei, W., Tang, X.T., and Dong, F. "Synthesis of MoS_2/g-C_3N_4 nanocomposites with enhanced visible-light photocatalytic activity for the removal of nitric oxide (NO)", *Opt. Express*, **24**(2), pp. 10205–10212 (2016).

14. Ye, Y., Zang, Z., Zhou, T., Dong, F., Lu, S., Tang, X., Wei, W., and Zhang, Y. "Theoretical and experimental investigation of highly photocatalytic performance of CuInZnS nanoporous structure for removing the NO gas", *J. Catal.*, **357**(152), pp. 100–107 (2018).

15. Huang, H., Zhang, J., Jiang, L., and Zang, Z. "Preparation of cubic Cu_2O nanoparticles wrapped by reduced graphene oxide for the efficient removal of rhodamine B", *J. Alloys Compd.*, **718**(204), pp. 112–115 (2017).

16. Zhu, W., Feng, X., Feng, L., and Jiang, L. "UV-Manipulated wettability between superhydrophobicity and super-hydrophilicity on a transparent and conductive SnO_2 nanorod film", *Chem. Commun*, **26**(8), pp. 2753–2755 (2006).

17. Krishna, M.G., Madhurima, V.D., and Purkayastha, D. "Metal oxide thin films and nanostructures for self-cleaning applications: current status and future prospects", *Eur. Phys. J. Appl. Phys.*, **62**(6), pp. 30001–6 (2013).

18. Miyauchi, M., Nakajima, A., Watanabe, T., and Hashimoto, K. "Photocatalysis and photoinduced hydrophilicity of various metal oxide thin films", *Chem. Mater.*, **14**(7), pp. 2812–2816 (2002).

19. Othmen, W.B.H., Sieber, B., Cordier, C., Elhouichet, H., Addad, A., Gelloz, B., Moreau, M., Barras, A., Ferid, M., and Boukherroub, R. "Iron addition induced tunable band gap and tetravalent Fe ion in hydrothermally prepared SnO_2 nanocrystals: Application in photocatalysis", *Mater. Res. Bull.*, **83**(1), pp. 481–490 (2016).

20. David, A.B. and Miller, G. "Multilayer thin-film coatings for optical communication systems", *Optical Society of America*, **5**(9), pp. 1–3 (2004).

21. Brsan, E. "Magnetic properties of multilayer thin film with ising-like ordering", *Acta Physica Polonica A*, **117**(3), pp. 500–503 (2010).

22. Solterbeck, C.H., Souni, M., and Iakovlev, S. "Multilayer ferroelectric thin films for pyroelectric applications", *Sensors and Actuators A*, **109**(1–2), pp. 114–119 (2003).

23. Sangchay, W., Sikong, L., and Kooptarnond, K. "Photochromic and self-cleaning properties of TiO_2-AgCl/TiO_2-xCu thin films", *Journal of Nanoscience and Nanotechnology*, **13**(2), pp. 1448–1452 (2013).

24. JCPDS data card No. 21-1250.

25. JCPDS (Joint Committee for Powder diffraction Standards), Data Cards, Swarthmore, PA, 41–1445 (1997).

26. Benhaoua, B., Abbas, S., Rahal, A., Benhaoua, A., and Aida, M.S. "Effect of film thickness on the structural, optical and electrical properties of SnO_2: F thin films prepared by spray ultrasonic for solar cells applications", *Superlattices Microstruct*, **83**(5), pp. 78–88 (2015).

27. Pavlopoulos, D., Khatiab, S.A., Button, T., and Abell, J. "Spray pyrolysis for the production of biaxially textured MgO thin films for second generation coated conductors", *Journal of Physics: Conference Series*, **97**(March 2008). DOI: https://doi.org/10.1088/1742-6596/97/1/012098

28. Babar, A.R., Shinde, S.S., Moholkar, A.V., Bhosale, C.H., Kim, J.H., and Rajpure, K.Y. "Phyicical properties of spayed antimony doped tin oxide thin films: the role of thickness", *J. Semicond.*, **32**(5), pp. 1–8 (2011).

29. Babar, A.R., Shinde, S.S., Moholkar, A.V., Bhosale, C.H., Kim, J.H., and Rajpure, K.Y. "Sensing properties of sprayed antimony doped tin oxide thin films: solution molarity", *J. Alloys Compd.*, **509**(5), pp. 3108–3115 (2011).

30. Elahi, M. and Ghobadi, N. "Structural, optical and electrical properties of CdSe nanocrystalline films", *Iranian Physical Journal*, **2**(1), pp. 27–31 (2008).

31. Yadav, A.A. and Salunke, S.D. "Properties of spray deposited nanocrystalline indium selenide", *J. Mater. Sci. Mater. Electron.*, **26**(8), pp. 5416–5425 (2015).

32. Yadav, A.A. "Nanocrystalline copper selenide thin films by chemical spray pyrolysis", *J. Mater. Sci. Mater. Electron.*, **25**(5), pp. 1251–1259 (2014).

33. Kilic, C. and Zunger, A. "Origins of coexistence of conductivity and transparency in SnO_2", *Physics Review Letters*, **88**(6), pp. 095501–6 (2002).

34. Nwodo, M.O., Ezugwu, S.C., Ezema, F.I., Asogwa, P.U., and Osuji, R.U. "Chemical bath deposition and characterization of PVP cappetin oxide tin films", *Journal of Optoelectronics and Biomedical Materials*, **2**(4), pp. 267–272 (2010).

35. Lin, H., Kumon, S., Kozuka, H., and Yoko, T. "Electrical properties of sol-gel-derived transparent titania films doped with ruthenium and tantalum", *Thin Solid Films*, **315**(1–2), pp. 266–272 (1998).

36. Bardeen, J., Blatt, F.J., and Hall, L.H. "Indirect transition from the valence to the conduction bands", *Proceeding of Conference on Photoconductivity*, pp. 149–154 (1965).

37. Tauc, J.C. "Optical properties of solid", F.A beles, North Holland Publishing, Amsterdam, p. 279 (1972).

38. Pankove, J.I., *Optical Processes in Semiconductor*, Dover Publication, Inc. New York., **3**, p. 34 (1971).

39. Shanthi, E., Dutta, V., Banerjee, A., and Chopra, K.L. "Electrical and optical properties of undoped and antimony-doped tin oxide films", *Journal of Applied Physics*, **51**(5), pp. 6243–625 (1980).

40. Afify, H.H., Momtaz, R.S., Badawy, W.A., and Nasser, S.A. "Some physical properties of fluorine-doped SnO_2 films prepared by spray pyrolysis", *Journal of Materials Science Materials in Electronics*, **2**(1), pp. 40–45 (1991).

41. Saipriya, S., Sultan, M., and Singh, R. "Effect of environment and heat treatment on the optical properties of RF-sputtered SnO_2 thin films", *Physica B*, **406**(56), pp. 812–817 (2011).

42. Igwe, H.U. and Ugwu, E.I. "Optical characteristics of nanocrystaline thermal annealed tin oxide (SnO_2) thin film samples prepared by chemical bath deposition technique", *Journal of Advance in Applied Science Research*, **1**(3), pp. 240–246 (2010).

43. Dubal, D.P., Dhawale, D.S., Salunkhe, R.R., Fulari, V.J., and Lokhande, C.D. "A novel chemical synthesis and characterization of Mn_3O_4 thin films for supercapacitor application", *J. Alloys Compd.*, **497**(85), pp. 166–170 (2010).

44. Lim, Y.C., Westerwalbesloh, T., Aschentrup, A., Wehmeyer, O., Haindl, G., Kleineberg, U., and Heinzmann, U. "Fabrication and characterization of EUV multilayer mirrors optimized for small spectral reflection bandwidth", *Appl. Phys. A*, **72**(5), pp. 121–124 (2001).

45. Morton, D.E. "Characterizing optical thin films (I)", *Vacuum Technology and Coating*, **2**(9), pp. 24–31 (2001).

46. Manifacier, J., De Murcia, C.M., Fillard, J.P., and Vicario, E. "Optical and electrical properties of SnO_2 thin films in relation to their stoichiometric deviation and their crystalline structure", *Thin Solid Films*, **41**(14), pp. 127–144 (1977).

47. Dhar Purkayastha, D., Ghanashyam Krishna, M., and Madhurima, V. "Molybdenum doped tin oxide thin films for self-cleaning applications", *Mater Lett*, **124**(52), pp. 21–24 (2014).

48. Dhar Purkayastha, D., Brahma, R., and Madhurima, V. "Effects of metal doping on photoinduced hydrophilicity of SnO_2 thin films", *Bulletin Mater Sci*, **38**(3) pp. 203–208 (2015).

49. Mane, R.S., Chang, J., Ham, D., Pawar, B.N., Ganesh, T., Cho, B.W., Lee, J.K., and Han, S.H. "Dye-sensitized solar cell and electrochemical supercapacitor applications of electrochemically deposited hydrophilic and nanocrystalline tin oxide film electrodes", *Curr. Appl. Phys.*, **9**(1), pp. 87–95 (2009).

Biographies

S.M. Alduwaib has been working at Mustansiriya University for 15 years as a teacher. He received his PhD in thin films from College of Science, Baghdad University in 2012. He studies the analysis and interpretation of electron microscope images of nanomaterials. He has practical experience in the field of maintenance and repair of industrial machines as well as electrical control. His current interests lies in developing clean energy sources as well as recycling materials.

Muhannad M. Abd received his PhD in Physics of Materials and is currently working as the manager of the Quality Assurance Department at Mustansiriyah University. He aims to author an encyclopedia in the science of nanomaterials. He has conducted many researches in the field of nanomaterials with many publications in the field of applying quality systems in academic work.

Ali Hussain Abdalrazzaq Jalaukhan was born in Holly Kerbala, Iraq in 1962. He received his BSc in Physics from University of Mosul, Iraq in 1983. His MSc in Solid State Physics is from University of Baghdad, Iraq in 1991. His thesis project was entitled "The Optical and Electrical Properties of Thin Films Compound $CuInSe_2$". His PhD project was entitled "Microstructure and Optoelectronics Characterizations of Ga_xSb_{1-x}/GaAs Heterojunction", conducted at Baghdad University completed in 2012. Then, he joined University of Kerbala as a teacher and a researcher. His current research is in the fields of thin films, characterization of carbon nanostructures, graphene nano plates, antibacterial studies, and self-cleaning applications. Jalaukhan has published 12 research papers in many conferences and journals.